Inorganic Chemistry

Article

pubs.acs.org/IC

Reactivity of a Series of Isostructural Cobalt Pincer Complexes with CO_2, CO, and H^+

David W. Shaffer,[†] Samantha I. Johnson,[‡,§] Arnold L. Rheingold,[∥] Joseph W. Ziller,[†] William A. Goddard, III,[‡,§] Robert J. Nielsen,[‡,§] and Jenny Y. Yang*[,†]

[†]Department of Chemistry, University of California, Irvine, 1102 Natural Sciences 2, Irvine, California 92697, United States

[‡]Joint Center for Artificial Photosynthesis, California Institute of Technology, Pasadena, California 91125, United States

[§]Department of Chemistry, California Institute of Technology, Pasadena, California 91125, United States

[∥]Department of Chemistry and Biochemistry, University of California, San Diego, La Jolla, California 92093, United States

Supporting Information

ABSTRACT: The preparation and characterization of a series of isostructural cobalt complexes $[Co(t\text{-}Bu)_2P^EPy^EP(t\text{-}Bu)_2(CH_3CN)_2][BF_4]_2$ (Py = pyridine, E = CH_2, NH, O, and X = BF_4 (**1a**–**c**)) and the corresponding one-electron reduced analogues $[Co(t\text{-}Bu)_2P^EPy^EP(t\text{-}Bu)_2(CH_3CN)_2][BF_4]_2$ (**2a**–**c**) are reported. The reactivity of the reduced cobalt complexes with CO_2, CO, and H^+ to generate intermediates in a CO_2 to CO and H_2O reduction cycle are described. The reduction of **1a**–**c** and subsequent reactivity with CO_2 was investigated by cyclic voltammetry, and for **1a** also by infrared spectroelectrochemistry. The corresponding CO complexes of (**2a**–**c**) were prepared, and the Co–CO bond strengths were characterized by IR spectroscopy. Quantum mechanical methods (B3LYP-d3 with solvation) were used to characterize the competitive reactivity of the reduced cobalt centers with H^+ versus CO_2. By investigating a series of isostructural complexes, correlations in reactivity with ligand electron withdrawing effects are made.

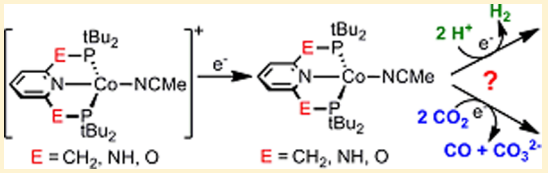

INTRODUCTION

There is great interest in using CO_2 as a feedstock for generating chemical fuels from renewable energy sources.[1] A potential high-value transformation is the two electron reduction of CO_2 to produce CO, which can be combined with H_2 generated from renewable sources[2] to produce liquid hydrocarbon fuels through industrial Fischer–Tropsch processes.[3] However, fast and efficient catalysts composed of abundant metals are still needed for the selective reduction of CO_2 to CO.[1f–k,4]

The Sabatier principle is effective at describing catalytic activity to guide the development of new catalysts.[5] This concept illustrates the importance of balancing substrate and product interaction at a catalyst active site in order to achieve high efficiency and reaction rate. The effect of maximizing substrate interaction while minimizing product interaction is often depicted as a volcano plot. We are interested in applying this principle, commonly used to describe catalytic activity relationships in heterogeneous systems, to the design of molecular transition metal catalysts for CO_2 reduction to CO. By adjusting the ligand properties, we can modify the energy of CO_2 binding and CO release at a single metal site.

For this study, a series of isostructural cobalt complexes using pincer ligands of varying electron withdrawing character was synthesized and studied. The complexes are shown in Chart 1. Cobalt complexes with these pincer ligands have been previously studied for their physical properties,[6] and recent work has focused on catalytic applications such as C–H activation,[7] borylation,[8] and olefin polymerization.[9] The combination of the pyridine backbone and phosphine arms provides stability toward reducing conditions. The meridional tridentate ligand scaffold leaves an open coordination site *trans* to the pyridine for CO_2 binding, which is reminiscent of triphosphine complexes that show catalytic activity for reduction of CO_2 to CO.[10] Additionally, the ligand variants with CH_2, NH, and O bridges between the pyridine and phosphine are readily synthesized and represent a stepwise increase in the electron withdrawing nature of the ligand without altering the primary coordination sphere. Although there are several examples of molecular cobalt complexes that have activity toward CO_2 reduction,[11] the use of these ligand environments has been minimally explored.[12]

Chart 1

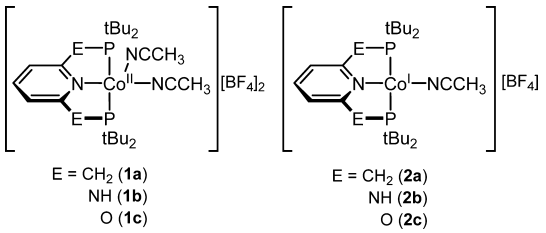

Received: September 8, 2014
Published: December 3, 2014

   dx.doi.org/10.1021/ic5021725 | *Inorg. Chem.* 2014, 53, 13031–13041

Reduction of CO_2 to CO requires formal loss of an O^{2-} dianion. In other examples of catalytic reduction, stoichiometric amounts of oxygen atom acceptors (i.e., diboron, borane, hydrosilane, or anhydrides) have been used to close the catalytic cycle.[13] However, the formation of strong bonds with oxygen acceptors precludes an efficient energy-storing catalytic cycle. An ideal scenario would utilize protons as a stoichiometric O atom acceptor to generate water, as shown in eq 1. However, this adds the complication of competitive proton binding at the reduced metal center and can result in reduction of protons instead of CO_2.[14] Therefore, we also examined the relationship between the redox properties of the complexes and pK_a of the reduced metal centers. The thermodynamic and kinetic parameters for CO_2, CO, and H^+ binding are all important considerations for selective catalyst design for the reaction shown in eq 1.

$$CO_2 + 2e^- + 2H^+ \rightarrow CO + H_2O \qquad E^{\circ\prime} = -0.53\ \text{V at pH 7 vs NHE} \qquad (1)$$

RESULTS AND DISCUSSION

Synthesis, Characterization, and Structural Studies of $[(P^EN^EP)Co(NCCH_3)_2][BF_4]_2$ (1a–c). The series of $[(P^EN^EP)Co(NCCH_3)_2][BF_4]_2$ (E = C, **1a**; N, **1b**; O, **1c**) complexes were prepared by addition of the free ligands to $[Co(NCCH_3)_6][BF_4]_2$. For all three ligands, addition of solid P^EN^EP to an acetonitrile solution of $[Co(NCCH_3)_6][BF_4]_2$ produced a dark orange solution. Removal of solvent *in vacuo* resulted in dark orange oils that precipitated the products as orange powders upon stirring in THF or benzene.

Two variations of the Co(II)–P^CN^CP tetrafluoroborate salt were obtained using different methods of recrystallization. Diffusion of pentane into a saturated dichloromethane solution produced orange crystals of the 5-coordinate cobalt complex with one acetonitrile ligand in the plane of the P^CN^CP ligand and an axial BF_4 with a Co–F distance of 2.3446(9) Å. The structure for this complex with the formula $[(P^CN^CP)Co(NCCH_3)(BF_4)][BF_4]$ is shown in Figure S1 in the Supporting Information. The value of τ_5 is 0.18, and the sum of the angles around the basal plane is 358.7°.[15] However, elemental analysis of crystals grown from acetonitrile/toluene solution was consistent with the formulation $[(P^CN^CP)Co(NCCH_3)_2][BF_4]_2$ (**1a**). The dibromide $(P^CN^CP)CoBr_2$ was also synthesized using $CoBr_2$ but isolated as the BPh_4 salt by treating it with 2 equiv of $NaBPh_4$ in CH_3CN, forming the analogous complex $[(P^CN^CP)Co(NCCH_3)_2][BPh_4]_2$ (**1a′**). The structure for this complex is shown in Figure 1. The metrical parameters of the BPh_4 salt, which are listed in Table 1, are similar to those of the BF_4-bound salt, with the obvious exception of those involving the pseudoaxial ligand.

X-ray quality crystals of **1b** were grown by slow evaporation of acetonitrile from an acetonitrile/toluene solution. The structure of the cationic cobalt complex of **1b**, which is shown in Figure 2, is similar to that of **1a′**, with the most notable difference being a bending of the apical $NCCH_3$ ligand away from the pyridine that is manifested in a larger N_{py}–Co–N_{axial} angle. The τ_5 value for **1b** is 0.08.[15] The reaction between P^ON^OP and $[Co(NCCH_3)_2][BF_4]_2$ (**1c**) proceeded similarly; however, attempts at growing X-ray quality crystals resulted in oils and decomposition products. One attempt resulted in a crystallographically charactarized macrocyclic $(P_2N_2)Co$ complex, possibly formed by nucleophilic attack of a $(O\text{-py-}O)^{2-}$ fragment on a $(P^ON^OP)Co$ complex. An analogous nickel example of the same decomposition pathway has been described.[16]

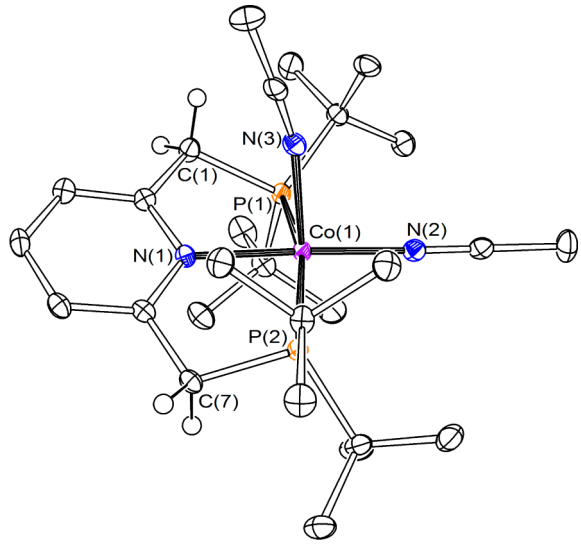

Figure 1. ORTEP diagram of $[(P^CN^CP)Co(NCCH_3)_2][BPh_4]_2$ (**1a′**). Ellipsoids are shown at 50% probability. Hydrogen atoms (except $-CH_2-$), a molecule of CH_3CN, and two BPh_4^- ions have been omitted for clarity.

Table 1. Selected Bond Distances (Å), Angles (deg), and τ_5 for $[(P^CN^CP)Co(NCCH_3)_2][BPh_4]_2$ (1a′), $[(P^NN^NP)Co(NCCH_3)_2][BF_4]_2$ (1b), and $[(P^NN^NP)Co(NCCH_3)][BF_4]$ (2b)[a]

	1a′	1b	2b
Co–N_{py}	1.9632(15)	1.9480(13)	1.925(3)
Co–P_1	2.2761(6)	2.2623(4)	2.1844(7)
Co–P_2	2.3030(6)	2.2893(4)	2.1843(7)
Co–L_{eq}	1.9002(16)	1.8963(13)	1.834(3)
Co–L_{ax}	2.0868(17)	2.0720(14)	
N_{py}–Co–L_{eq}	176.97(7)	168.50(5)	177.68(13)
P–Co–P	160.17(2)	163.416(17)	168.67(4)
τ_5	0.28	0.08	

[a] L_{eq} and L_{ax} indicate the donor atoms of the ligands best described as *trans* and *cis*, respectively, from the pyridine donor N. **2b** contains 4 cobalt molecules in the asymmetric unit. Parameters listed above are for a representative molecule in the asymmetric unit cell.

Magnetic Properties of $[(P^EN^EP)Co(NCCH_3)_2][BF_4]_2$ (1a–c). The spin states of the complexes were experimentally determined to facilitate the computational studies. EPR spectra at 77 K for **1a–c** are indicative of low-spin, $S = {}^1/_2$ systems (shown in Figure 3). EPR spectra **1a** and **1b** were taken in frozen EtOH solutions; **1c** is unstable in EtOH, so its spectrum was collected in 1:1 CH_3CN/THF. The signals for **1a–c** were centered at g = 2.28, 2.26, and 2.24, respectively, with hyperfine coupling to the cobalt center of 94, 91, and 85 G, respectively. The same spin state is observed at room temperature using the Evans method measurements for complexes **1a–b** in CD_3CN (5% C_6H_6 as an internal reference). The magnetic moments (2.0 μ_B) contrast with the high spin $S = {}^3/_2$ systems observed for $(Ph\text{-}P^CN^CP)CoX_2$ salts (X = Cl, Br, NO_3; 4.3–4.7 μ_B), reflecting the stronger field nature of the acetonitrile ligands.[6a,17]

dx.doi.org/10.1021/ic5021725 | Inorg. Chem. 2014, 53, 13031–13041

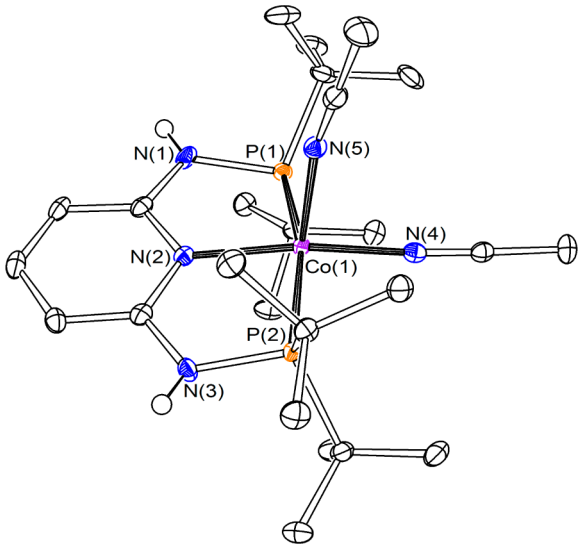

Figure 2. ORTEP diagram of $[(P^{N}N^{N}P)Co(NCCH_3)_2][BF_4]_2$ (**1b**). Ellipsoids are shown at 50% probability. Hydrogen atoms (except N–H), a molecule of CH_3CN, and BF_4^- ions have been omitted for clarity.

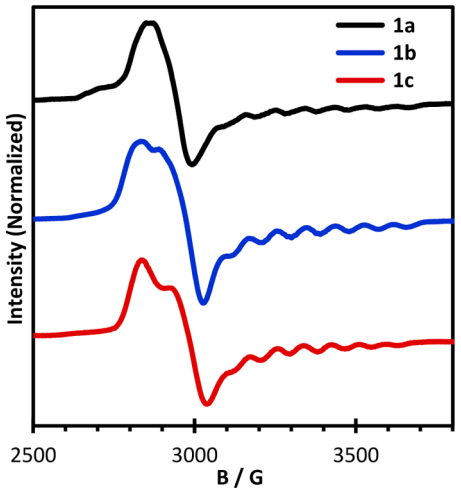

Figure 3. EPR spectra for $[(P^{E}N^{E}P)Co(NCCH_3)_2][BF_4]_2$ (E = C, **1a**, top/black; N, **1b**, middle/blue) in EtOH at 77 K and $[(P^{O}N^{O}P)Co(NCCH_3)_2][BF_4]_2$ (**1c**, bottom/red) in 1:1 CH_3CN/THF.

Electrochemical Studies of $(P^{E}N^{E}P)Co(NCCH_3)_2][BF_4]_2$ (1a–c). Cyclic voltammetry of **1a–c** (shown in Figure 4) reveals two reduction events. The first reduction, assigned to the Co(II/I) couple (*vide infra*), is reversible ($E_{1/2}$ values are listed in Table 2). This couple becomes more positive from **1a**, **1b**, to **1c**, which is the expected trend as the pincer ligand becomes more electron withdrawing (E = CH_2, NH, O) in this isostructural series. The first reductions of **1a–c** display diffusion-controlled behavior (linear relationship between i_p vs $\nu^{1/2}$, ν = scan rate) for scan rates from 0.025 V/s to 1.60 V/s (see Figure S2 in the Supporting Information).

In the same range of scan rates, the second reduction for **1a–c** is completely irreversible (see Supporting Information Figure S3). Although reduced $P^{C}N^{C}P$ cobalt complexes are known to exhibit ligand noninnocence,[6d,18] no redox potential shifts are observed in the reduction of **1a–c** for the scan rates investigated (25–1600 mV/s), indicating no chemical change on the electrochemical time scale. However, because of the possibility of ligand redox noninnocence, we have not formally assigned the reduction to a metal centered Co(I/0) event. No trend correlates these reduction potentials with the electronic nature of the ligand; however, as the reduction is not reversible, the observed onset potential may not accurately reflect $E_{1/2}$.

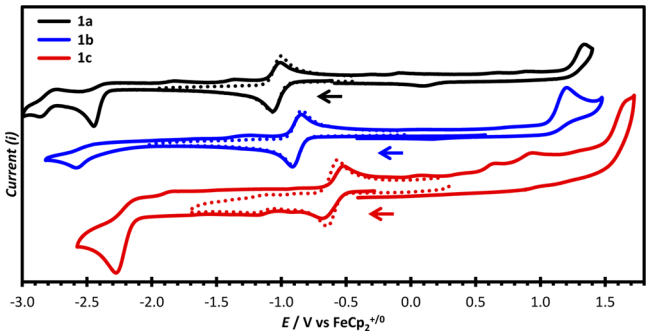

Figure 4. Cyclic voltammograms of $[(P^{E}N^{E}P)Co(NCCH_3)_2][BF_4]_2$ (E = C, **1a**, top, black; N, **1b**, middle, blue; O, **1c**, bottom, red). 1.0 mM analyte in CH_3CN with 0.20 M Bu_4NPF_6 at 100 mV/s. Isolation of the first reduction event is indicated by dotted lines. Arrows indicate scan direction and resting potential.

Table 2. Redox Potentials versus $Fe(Cp)_2^{+/0}$ for $[(P^{E}N^{E}P)Co(NCCH_3)_2][BF_4]_2$ (E = C, 1a; N, 1b; O, 1c)

compd	E_{pc}(red3)	E_{pc}(red2)	$E_{1/2}$(red1)	E_{pa}(ox)
1a	−2.83	−2.45	−1.03	1.33
1b		−2.56	−0.88	1.20
1c		−2.27	−0.61	

Complexes **1a** and **1b** have irreversible oxidations at 1.33 and 1.20 V, respectively, but **1c** displays no oxidation within the limits of the solvent window.

Synthesis and Characterization of $[(P^{E}N^{E}P)Co(NCCH_3)][BF_4]$ (2a–c). The reversible nature of the Co(II/I) couples indicates that the corresponding Co(I) complexes should be stable and isolable. Chemical reductions were carried out to isolate the $[(P^{E}N^{E}P)Co]^+$ complexes. Treatment of $[(P^{C}N^{C}P)Co(NCCH_3)_2][BF_4]_2$ (**1a**) with 1 equiv of KC_8 in THF/CH_3CN at ca. 200 K produced a dark green solution. Filtration, solvent removal, and washing the resulting solid with diethyl ether gives $[(P^{C}N^{C}P)Co(NCCH_3)][BF_4]$ (**2a**) in 89% yield. Complex **2a** is diamagnetic and displays a ^1H NMR spectrum in CD_3CN with resonances at 7.46 ppm (triplet) and 7.08 ppm (doublet) corresponding to the aromatic protons, 3.11 ppm (singlet) corresponding to the methylene groups, and 1.48 ppm (broad singlet) corresponding to the *tert*-butyl groups. A peak for the coordinated acetonitrile ligand is not observed presumably due to exchange with the deuterated solvent. A very broad resonance at 103.0 ppm in the ^{31}P NMR spectrum is assigned to the phosphorus atom in the ligand. The infrared absorption spectrum of solid **2a** reveals an absorption feature at 2229 cm^{-1}, attributed to the coordinated acetonitrile. Single crystals of **2a** were grown by evaporation of CH_3CN from a CH_3CN/toluene solution and evaluated by X-ray crystallography. The resulting structure confirmed the connectivity as 4-coordinate $[(P^{C}N^{C}P)Co(NCCH_3)][BF_4]$ and is shown in Supporting Information Figure S10; however, the data was not of high enough quality for a refined structure. The formulation was also supported by atmospheric-pressure chemical ionization mass spectrometry (APCI-MS), which displayed peaks at m/z of 495.4 and 454.4, corresponding to

dx.doi.org/10.1021/ic5021725 | *Inorg. Chem.* 2014, 53, 13031–13041

$[(P^CN^CP)Co(NCCH_3)]^+$ and $[(P^CN^CP)Co]^+$, respectively, and no peak corresponding to $[(P^CN^CP)Co(NCCH_3)_2]^+$.

$[(P^NN^NP)Co\text{-}(NCCH^3)][BF_4]$ (**2b**) was obtained in a procedure similar to that of **2a**. Treatment of a solution of **1b** in THF/CH_3CN with 1 equiv of KC_8 caused a color change from dark orange to dark purple. Filtration, removal of solvent, and washing with diethyl ether provides **2b** in 93% yield. The ^1H NMR of **2b** in CD_3CN contains peaks at 7.16 ppm (triplet) and 6.01 ppm (doublet) corresponding to the aromatic protons and a broad singlet at 1.47 ppm corresponding to the *tert*-butyl group. The N−H protons appear as a broad singlet at 6.48 ppm. The ^{31}P NMR spectrum displays a broad peak at 121.0 ppm. The IR absorption spectrum of solid **2b** displays a clear N−H stretch at 3322 cm^{-1} and a peak at 2213 cm^{-1} attributed to the coordinated acetonitrile. APCI-MS verified the formulation of **2b**, exhibiting peaks at 497.4 and 456.3, corresponding to $[(P^NN^NP)Co(NCCH_3)]^+$ and $[(P^NN^NP)Co]^+$, respectively. No significant peak was observed corresponding to $[(P^NN^NP)Co(NCCH_3)_2]^+$. Crystals of sufficient quality for analysis by X-ray diffraction were grown by cooling a saturated CH_3CN/toluene solution to 238 K. The structure, shown in Figure 5, reveals a square-planar geometry around the

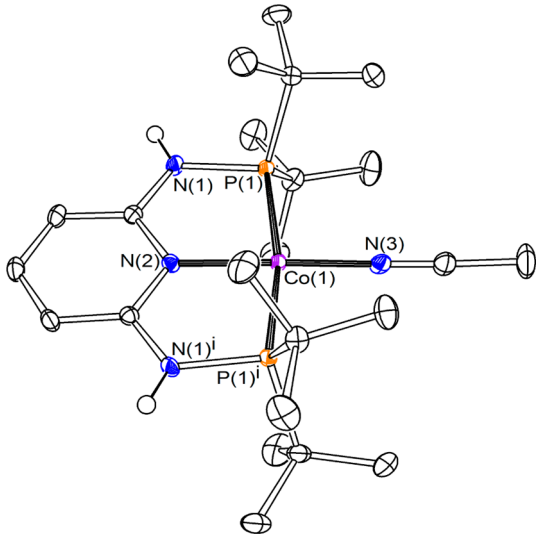

Figure 5. ORTEP diagram of one of four molecules in the asymmetric unit $[(P^NN^NP)Co(NCCH_3)][BF_4]$ (**2b**). Ellipsoids are shown at 50% probability. Hydrogen atoms (except N−H) and a BF_4^- ion have been omitted for clarity.

cobalt(I) center, with the angles around the metal center summing to 360.2°. Shorter metal−ligand bond distances relative to **1b** are consistent with stronger π-bonding for the more electron-rich metal center. Elemental analysis of these crystals confirmed the formulation as $[(P^NN^NP)Co(NCCH_3)][BF_4]$.

Complex **2c** was synthesized by stirring the free P^ON^OP ligand with $[Co(NCCH_3)_6][BF_4]_2$ in THF/CH_3CN, followed by cooling to 238 K and addition of an equivalent of KC_8. The dark purple product, **2c**, was filtered, washed with diethyl ether, and isolated in 72% yield. The ^1H NMR spectrum displayed aromatic peaks at 7.67 ppm (triplet) and 6.55 ppm (doublet) and a *tert*-butyl resonance at 1.56 ppm. The solid state IR spectrum exhibits a peak at 2250 cm^{-1}. The formulation of **2c** was also supported by APCI-MS, which contained peaks at m/z of 499.3 and 458.3, corresponding to $[(P^ON^OP)Co(NCCH_3)]^+$ and $[(P^ON^OP)Co]^+$, respectively, and no peak corresponding to $[(P^ON^OP)Co(NCCH_3)_2]^+$.

Electrochemical Reduction of $[(P^EN^EP)Co(NCCH_3)_2][BF_4]_2$ (1a−c) under 1 atm CO_2. The reactivity of CO_2 with the reduced forms of **1a−c** was examined by cyclic voltammetry in CO_2-saturated acetonitrile. Figure 6 displays

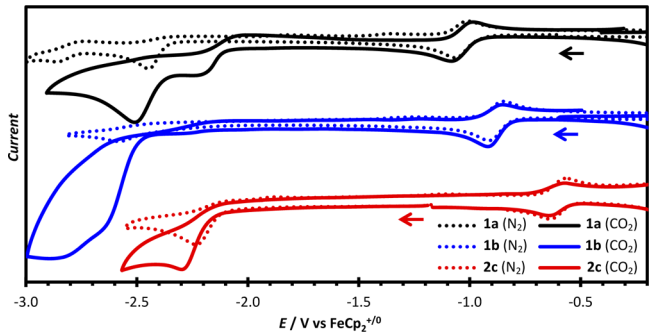

Figure 6. Cyclic voltammograms of $[(P^EN^EP)Co(NCCH_3)_2][BF_4]_2$ (E = C, **1a**, top, black; N, **1b**, middle, blue) and $[(P^ON^OP)Co(NCCH_3)][BF_4]$ (**2c**, bottom, red) under N_2 (dotted lines) and CO_2 (solid lines). 1.0 mM analyte in CH_3CN with 0.20 M Bu_4NBF_4 at 100 mV/s. Arrows indicate the scan direction and the resting potential.

voltammograms of **1a−b** and **2c** under nitrogen (dotted lines) and carbon dioxide (solid lines). Due to the instability of **1c** (which slowly decomposed in solution), **2c** was used in its place for electrochemical reactivity experiments. For all three compounds there is no difference in the Co(II/I) couple between the voltammograms under CO_2 versus N_2, remaining fully reversible at scan rates from 0.0125 to 1.6 V/s (shown in Figure S4 in the Supporting Information), indicating the Co(I) complexes are unreactive to CO_2. This was confirmed by adding CO_2 to **2a**; after 10 min, the ^1H and ^{31}P NMR spectra exhibited no observable change.

The second reduction for **1a−c**, on the other hand, exhibits significantly different behavior in the presence of CO_2, displaying a positive shift in the reduction potential that varies with scan rate and ligand substituent. For **1a**, at slower scan rates, the second reductive wave under CO_2 appears positive relative to that under N_2. Figure 7, left, shows cyclic voltammograms of **1a** under CO_2 at different scan rates (ν), normalized by dividing the current by $\nu^{-1/2}$. Two peaks in the cathodic current are observed (in addition to the reversible first reduction): the first at approximately −2.2 V, and the second at approximately −2.5 V (similar to the potential under N_2). At scan rates ≤125 mV/s, the former shows some reversibility, whereas the more negative reduction is irreversible at all scan rates. The shift in reduction potential relative to the reduction under N_2 reaches a maximum of 300 mV at the slowest scan rate of 12.5 mV/s. At sufficiently fast scan rates (≥800 mV/s), no significant shift in potential is observed, though the magnitude of the wave at −2.5 V is greater. For **1b**, a similar positive shift is observed in the presence of CO_2, but without a distinct maximum in i_{pc} even at scan rates as slow as 12.5 mV/s. Figure 7, middle, shows cyclic voltammograms of **1b** under CO_2 at different scan rates (ν) normalized by $\nu^{-1/2}$. At slow scan rates (≤25 mV/s), the second reduction of **1b** contains a feature with an onset potential of approximately −2.2 V and an irreversible peak at −2.7 V. At 12.5 mV/s, a maximum shift of approximately 200 mV was observed for the new feature relative to the reduction under N_2. At scan rates faster than 200

dx.doi.org/10.1021/ic5021725 | Inorg. Chem. 2014, 53, 13031−13041

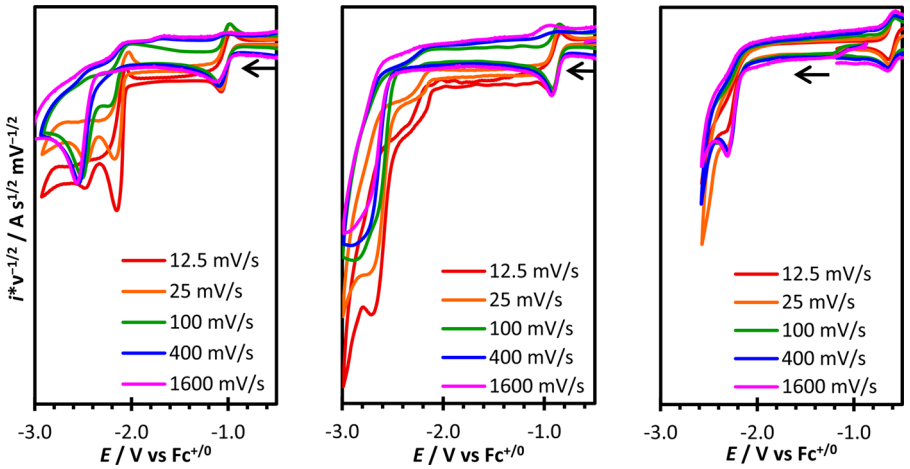

Figure 7. Cyclic voltammograms of $[(P^{E}N^{E}P)Co(NCCH_3)_2][BF_4]_2$ (E = C, **1a**, left; N, **1b**, middle) and $[(P^{O}N^{O}P)Co(NCCH_3)][BF_4]$ (**2c**, right) at varying scan rates under CO_2, normalized by dividing the current by $\nu^{1/2}$. 1.0 mM analyte in CH_3CN with 0.20 M Bu_4NBF_4. Arrows indicate the scan direction and the position of the bulk material.

mV/s, no distinct shift was observed. The cyclic voltammograms for **2c** do not show any scan rate dependent reactivity under CO_2 at scan rates as low as 12.5 mV/s, shown in Figure 7, right.

Unlike other molecular cobalt-based CO_2 reduction catalysts, the Co(I) complexes display no reactivity with CO_2.[11f–i] This was observed electrochemically for all of the complexes, and confirmed by NMR for **2a**. However, reactivity with CO_2 is observed at the second reduction event, and was examined in more detail using scan rate dependent cyclic voltammetry. The positive potential shift with decreasing scan rate is consistent with a fast following reaction after the second reduction (kinetic potential shift). Since the concentration of saturated CO_2 in acetonitrile[19] is over 100-fold higher than the complex in our experimental conditions, the reaction was modeled using pseudo-first-order kinetics. We attempted to model the potential shift to obtain exact kinetic parameters for the reaction with CO_2 using DigiElch software. However, the added complication of the irreversible electron transfer step with an irreversible chemical step made extraction of exact kinetic information difficult. Using eq 2[20] for a first order chemical step following an electron transfer, we have estimated k_f to be about 10^{2-3} s^{-1} for the reaction of reduced **1a** and **1b** with CO_2 (ΔE = potential shift, ν = scan rate).

$$\Delta E = -\frac{RT}{nF}\left[0.780 + \frac{1}{2}\ln\frac{nF\nu}{(kf)RT}\right] \quad (2)$$

Notably, **1c**, with the most positive reduction potential, does not give a discernible kinetic potential shift with CO_2, even at the slowest scan rates. Prior analysis of single metal site reactivity toward CO_2 points toward a correlation between reduction potential and activation of CO_2.[14,21] The complexes support this trend since the complex with the most positive reduction potential (**1c**) shows slow or no reaction with CO_2, and the more negative reduction potentials in **1a** and **1b** are concomitant with more favorable reactivity toward CO_2.

Spectroelectrochemical Investigation of the CO_2 Activation Product. The reaction of the reduced complex **1a** with CO_2 was investigated by infrared spectroelectrochemistry. A −2.20 V potential was applied to a CO_2-saturated acetonitrile solution of 1.0 mM **1a** containing 0.20 M Bu_4NPF_6, and 1.0 mM ferrocene, and the difference infrared absorption spectra was measured over 12 min. Figure 8 shows the C−O double- and triple-bond region of the spectra over the course of the experiment. As the sample was electrolyzed, a peak grew in at 1921 cm^{-1}. Isotopically labeled $^{13}CO_2$ was used to authenticate that the observed stretch is a result of CO_2 reduction. When the identical experiment was performed with $^{13}CO_2$, the observed peak shifted to 1876 cm^{-1}. This is consistent with the value predicted for a CO bond based on a simple harmonic oscillator.

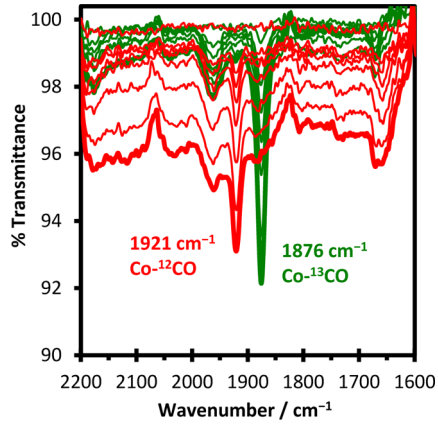

Figure 8. Spectroelectrochemical infrared difference spectra of $[(P^{C}N^{C}P)Co(NCCH_3)_2][BF_4]_2$ (**1a**) under natural abundance CO_2 (red lines) and $^{13}CO_2$ (green lines). 1.0 mM analyte in CH_3CN with 0.20 M Bu_4NPF_6.

The CO adduct of **2a**, $[(P^{C}N^{C}P)Co(CO)][BF_4]$, was independently prepared, and solution based IR measurements matched the stretch observed in the spectroelectrochemical experiment (*vide infra*). The initial product for the reaction of CO_2 with the two-electron reduced complex is expected to be a metal carboxylate. However, metal carboxylates at basic metal centers can reductively disproportionate to CO and CO_3^{2-}.[22] In essence, a second equivalent of CO_2 is acting as the oxygen atom acceptor for the initial CO_2 reduction to CO. This would result in the Co(II) carbonyl complex, which is easily reducible under the experimental conditions to the experimentally observed Co(I) carbonyl.

dx.doi.org/10.1021/ic5021725 | *Inorg. Chem.* 2014, 53, 13031−13041

Reaction of $[(P^ENP^E)Co(NCCH_3)][BF_4]$ (2a−c) with CO. The Sabatier principle describes the importance of both substrate activation and product release for catalysis. This is particularly important as CO is a much better ligand than CO_2 for most metal complexes, but must dissociate for the catalyst to turn over. To investigate the CO binding interaction, the cobalt(I) complexes $[(P^ENP^E)Co(NCCH_3)][BF_4]$ (**2a−c**) were treated with CO and the resulting products characterized by ^1H NMR, ^{31}P NMR, and IR spectroscopies. In CD_3CN, solutions of **2a−c** were bubbled with CO under 1 atm to produce new diamagnetic products. Only **2a** produced a single product, assigned as $[(P^CN^CP)Co(CO)][BF_4]$. For **2a**, the ^1H NMR spectrum of the resulting orange solution indicates clean conversion to a new product with aromatic peaks at 7.72 ppm (triplet) and 7.36 ppm (doublet). The methylene and *tert*-butyl peaks both appear as virtual triplets at 3.86 and 1.42 ppm. The ^{31}P NMR spectrum displays a single peak at 106.3 ppm. The thin film IR absorption spectrum of $[(P^CN^CP)Co(CO)][BF_4]$ displayed a carbonyl absorption at 1911 cm^{-1}. When taken as a solution droplet with 0.2 M Bu_4NBF_4 in CH_3CN, the carbonyl absorption was observed at 1920 cm^{-1}, consistent with the product in the IR spectroelectrochemical experiment described above.

Unlike **2a**, treatment of CD_3CN solutions of **2b** and **2c** with CO produced mixtures of two products which were observed by ^1H and ^{31}P NMR spectroscopy. Bubbling CO through a dark purple solution of **2b** in CD_3CN in a septum-capped NMR tube produced a green solution. The ^1H NMR spectrum of this solution appears to contain a single set of resonances analogous to those obtained from **2a**. A broad triplet at 7.45 ppm and a doublet at 6.35 ppm are consistent with the aromatic backbone protons, a broad singlet at 6.99 ppm is consistent with the N−H resonance, and the *tert*-butyl resonance appears as a virtual triplet at 1.44 ppm. The ^{31}P NMR spectrum, however, contains two broad peaks at 158.9 and 142.2 ppm, suggesting the presence of two species with overlapping ^1H NMR signals. No remaining **2b** was detected. The infrared absorption spectrum of this solution taken as an evaporated thin film displays a single strong absorption in the carbonyl region at 1923 cm^{-1} consistent with a cobalt(I)−carbonyl stretch, a very weak additional absorption at 1877 cm^{-1}, and a single broad N−H stretch at 3303 cm^{-1}. Analogous treatment of a CD_3CN solution of **2c** with CO resulted in an immediate color change from dark purple to green, and like **2b**, the starting material was completely consumed. The resulting ^1H and ^{31}P NMR spectra contained resonances corresponding to two different products. In the ^1H NMR spectrum, two sets of P^ON^OP resonances are clearly represented by two broad triplets at 8.10 and 7.95 ppm, overlapping doublets at 7.0 ppm, and a distorted broad virtual triplet at 1.54 ppm. The products appear in a ratio of approximately 0.6:1.0. The ^{31}P NMR spectrum contains broad peaks at 238.1 and 229.7 ppm. Thin film IR absorption reveals a single strong absorption in the carbonyl region at 1936 cm^{-1} and a weak but sharp signal at 1901 cm^{-1}.

On the basis of the major carbonyl stretch, the Co−CO bond varies in strength by **2a** > **2b** > **2c**. The increasing electron-withdrawing character of the ligands from CH_2 to NH to O substitution is manifested in the CO stretching frequency in addition to the potential of the cobalt(II/I) couple. The major CO infrared stretch increases from E = CH_2 (1911 cm^{-1}) to E = NH (1923 cm^{-1}) to E = O (1936 cm^{-1}). The increase in CO bond strength indicates less electron density at the metal for π-back bonding and a more weakly bound M−CO. This presents a dichotomy where metal centers with more negative reduction potentials are more favorable toward CO_2 activation, but in turn also have a stronger association with the product. This relationship has also been observed in heterogeneous systems by Norskov et al., where the scaling relationships for CO_2 activation and CO release are directly correlated, making catalyst optimization at single metal sites difficult.[23]

Electrocatalytic Studies. To test for electrocatalytic activity, **1a** was titrated with proton sources and studied by cyclic voltammetry and controlled-potential electrolysis. Cyclic voltammetry during titration of **1a** with triethylammonium tetrafluoroborate (pK_a = 18.8 in CH_3CN)[24] resulted in a minor increase in current relative to the acid without complex (see Figure S5 in the Supporting Information). The much weaker acid $[HDBU][BF_4]$ was then used (DBU = 1,8-diazabicyclo[5.4.0]undec-7-ene, pK_a = 24.3 in CH_3CN)[24] in an attempt to avoid protonation of the reduced cobalt complex.[25] This resulted in a current enhancement under N_2, which increased under 1 atm of CO_2, as shown in Figure 9.

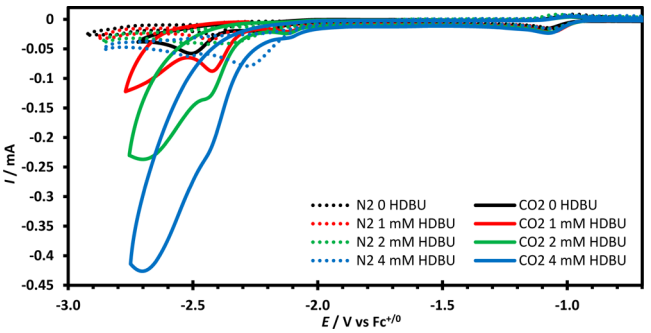

Figure 9. Cyclic voltammograms of $[(P^CN^CP)Co(NCCH_3)_2][BF_4]_2$ (**1a**) titrated with $[HDBU][BF_4]$ (0 mM, black; 1 mM, red; 2 mM, green; 4 mM, blue) under N_2 (dotted lines) and CO_2 (solid lines). 1.0 mM analyte and $FeCp_2$ internal reference in CH_3CN with 0.20 M Bu_4NPF_6 at 100 mV/s.

Bulk electrolysis was performed with **1a** (1.0 mM) and $[HDBU][BF_4]$ (50 mM) in CO_2-saturated CH_3CN solution at −2.15 V versus $Fe(Cp)_2^{+/0}$ for 1 h. During electrolysis, the orange solution changed to dark blue-green (consistent with **2a**). GC−MS analysis of the headspace detected H_2, but no reduced carbon-containing products.

Competitive Protonation of Reduced $[(P^ENP^E)Co(NCCH_3)_2][BF_4]_2$ (1a−c). An external proton source is necessary to complete CO_2 reduction to CO and H_2O. However, addition of protons provides a competitive pathway for proton reduction to generate hydrogen. The expected pathway for the latter would involve protonation at the reduced metal center to give a metal hydride intermediate.[26]

The basicity of cobalt(I) complex **2a** was estimated using cyclic voltammetry. The reversibility of the cobalt(II/I) couple ($i_{pc}/i_{pa} \approx 1$) was observed as sequentially stronger acids were added (see Supporting Information Figure S6). The reduction remains reversible after the addition of 1 equiv of [HDMF][OTf] (DMF = dimethylformamide, OTf = trifluoromethanesulfonate, pK_a = 6.1 in CH_3CN).[27] These results suggest that the pK_a of a protonated $[(P^CN^CP)Co^{III}H]^{+2}$ is less than ∼6. An NMR scale experiment in which slightly less than 1 equiv of $HBF_4{\cdot}OEt_2$ (pK_a = 1.8 ± 1.5 in CH_3CN)[28] was added to **2a** in CD_3CN cleanly produced peaks consistent with a $[(P^CN^CP)Co^{III}H]^{2+}$, placing a lower bound on the pK_a of ∼3.[29]

dx.doi.org/10.1021/ic5021725 | *Inorg. Chem.* 2014, 53, 13031−13041

Overall, the pK_a of the reduced cobalt complexes was difficult to experimentally measure due to complex instability. Therefore, quantum mechanical methods (B3LYP-d3 including PBF continuum solvation) were employed to gauge the relative energies of intermediates involved with CO_2 and H^+ reduction pathways for the most electron donating and withdrawing ligands, P^CN^CP and P^ON^OP. Free energies for the reaction of solvento complexes with CO_2 and protons can be seen in Scheme 1. For both ligands, the Co(I) and Co(II) complexes

Scheme 1. Calculated pK_a Values and CO_2 Binding Energies for the Reduction of 1a and 1c[a]

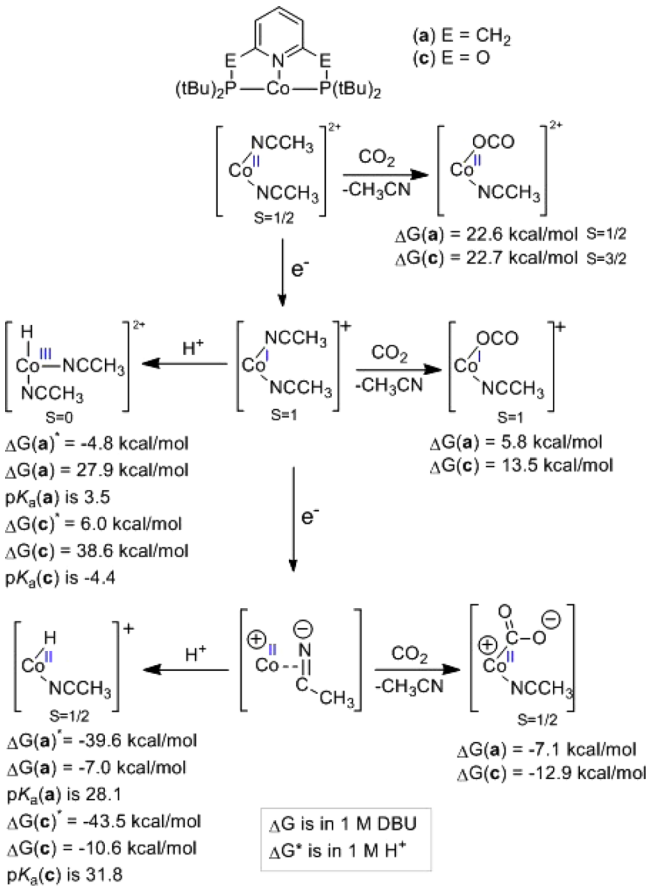

[a] ΔG energies are calculated in 1 M DBU, ΔG^* in 1 M H^+, both in CH_3CN. Potentials reported with respect to $FeCp_2^{+/0}$.

lowest in free energy contain two acetonitrile molecules. The second solvent molecule is weakly bound by 2.2 kcal/mol for the P^ON^OP (**2c**) complex. It is thermodynamically unfavorable by >20 kcal/mol for the Co(II) complexes (**1a** and **1c**) to lose one acetonitrile ligand and react with CO_2. The high-energy complex loosely binds CO_2 at the equatorial position through the oxygen. In the P^CN^CP complex, the Co−O bond length is calculated to be 2.10 Å, and in P^ON^OP complex the bond length is 2.12 Å.

It is also unfavorable for Co(I) (**2a** and **2c**) to react with CO_2, and only weakly coordinated complexes form, similar to the Co(II) case. Protonation of Co(I) by $HDBU^+$ is also highly endergonic. However, protonation to form $[(P^CN^CP)Co^{III}H(NCCH_3)_2]^{+2}$ from **2a** is accessible with strong acids, giving a calculated pK_a of 3.5, close to the value experimentally measured above. However, **2c** is calculated to be much less basic, and protonation is not possible in CH_3CN. These results are consistent with our experimental observations.

At more negative potentials, the Co(I) cations can be further reduced, as seen experimentally. In both P^CN^CP and P^ON^OP complexes, two kinds of low-energy, formally Co(0) structures were identified. When zero, one, or two acetonitrile molecules are coordinated to a neutral $(P^CN^CP)Co$ moiety through nitrogen, the wavefunction consists of a triplet Co(I) cation antiferromagnetically coupled to a radical anion ligand with spin distributed around the pyridine ring. The P^CN^CP ligands can thus become "redox active",[6d,18] but not under conditions for neutral-pH, low-overpotential CO_2 reduction. A few kcal/mol lower in free energy, however, lie neutral $(P^CN^CP)Co(\eta^2\text{-}NCCH_3)$ complexes incorporating a π-bound acetonitrile molecule. The Mulliken population on bound CH_3CN (−0.75 e^-) and C−N and Co−C bond lengths (1.23 and 1.95 Å, respectively) suggest the description of a η^2 π-bound Co(II) metallacycle. Preference for this mode of acetonitrile binding has been observed on other reducing (low oxidation state) metal centers.[30] The existence of isomers with various modes of solvent coordination within 8 kcal/mol of this ground state underscores the fluxional coordination at the reduced metal.

The quantum mechanical studies suggest that the neutral complexes should favorably react with CO_2 by 7.1 and 12.9 kcal/mol for the P^CN^CP and P^ON^OP complexes, respectively. This mirrors the experimental findings which indicate reactivity with CO_2 after reducing the Co(I) complex. In contrast to **2a**, the cyclic voltammogram of **2c** did not exhibit a kinetic potential shift with low scan rates upon reduction of **2c**, indicating a slower reaction with CO_2. However, an increase in current is observed under CO_2, indicating the reaction does proceed, to an extent, on the electrochemical time scale.

With the extra electron density provided by the second reduction, the lone pair from Co is donated into the π^* orbital of the CO_2, bending the C-bound CO_2 adduct. This is similar to the bonding that occurs with the bent CH_3CN adduct. The competing reaction with protons is also favorable. At pH = 24.3, reaction with protons is exergonic by 7.0 kcal/mol for the P^CN^CP complex, and 10.6 kcal/mol for the P^ON^OP complex.

CONCLUSION

The reduction and reactivity with CO_2, CO, and H^+ were examined using experimental and quantum mechanical methods for a series of isostructural cobalt complexes with stepwise changes in the electronic structure. These substrates are important because the design of selective CO_2 to CO and H_2O reduction catalysts involves the competitive reaction of CO_2 over H^+ at reduced metal centers and facile removal of the CO product.

Previous experimental studies have indicated that both CO_2 binding *and* protonation become more energetically favorable with increasing metal basicity, which is also observed with these complexes.[22d,31] An important result is that while the free energy of protonation can be tuned by adjusting the pK_a of the acid, this has only a minimal effect on the free energy of CO_2 binding.

In the case of these complexes, the acid used in the electrolysis studies, $[HDBU][BF_4]$ (pK_a = 24.3[24] in CH_3CN), was insufficiently weak to prevent protonation at the metal centers. A much weaker acid (pK_a > 36 in CH_3CN) would be necessary to avoid competitive hydrogen formation. However, metal centers with lower pK_a values would allow the use of

dx.doi.org/10.1021/ic5021725 | Inorg. Chem. 2014, 53, 13031−13041

weaker acids to circumvent a hydrogen production pathway, a strategy that has been demonstrated for another transition metal electrocatalyst.[25]

EXPERIMENTAL SECTION

Synthetic Methods and Materials. The complexes described below are air- and moisture-sensitive, and must be handled under an inert atmosphere of nitrogen using standard glovebox and Schlenk techniques. Unless otherwise noted, all procedures were performed at ambient temperature (21−24 °C). All solvents were sparged with argon and dried using a solvent purification system. Halocarbon solvents were passed through packed columns of neutral alumina and Q5 reactant. Acetonitrile, ethereal, and halogenated solvents were passed through two columns of neutral alumina. DMF and alcohol solvents were passed through columns of activated molecular sieves. The ligands P^CN^CP, P^NN^NP, and P^ON^OP and the cobalt starting material $[Co(NCCH_3)_6][BF_4]$ were synthesized according to established procedures.[32] Potassium graphite (KC_8) was synthesized by heating stoichiometric amounts of potassium and graphite in a sealed, evacuated Schlenk flask until a homogeneous bronze-colored powder was obtained. Triethylamine was freeze−pump−thawed three times and dried over molecular sieves. Graphite was dried under vacuum at 150 °C. All other materials, including CO_2 (99.999%) and CO (99.5%), were purchased from commercial sources and used without further purification.

Physical Methods. Elemental analyses (EA) were performed by Robertson Microlit Laboratories or on a PerkinElmer 2400 Series II CHNS/O analyzer. Electrospray ionization mass spectrometry (ESI-MS) and atmospheric-pressure chemical ionization mass spectrometry (APCI-MS) were performed with a JEOL JMR-600H mass spectrometer or a Waters LCT Premier mass spectrometer. Gas chromatography (GC) was performed on an Agilent Technologies 7890A GC system with front and back TCD channels. Nuclear magnetic resonance (NMR) spectra were recorded on a Bruker DRX500 spectrometer with a TCI cryoprobe (^{1}H and ^{13}C) or a DRX400 with a switchable QNP probe (^{1}H and ^{31}P) in dry, degassed solvents. ^{1}H NMR spectra were referenced to TMS using the residual proteo impurities of the solvent, ^{13}C NMR spectra were referenced to TMS using the natural abundance ^{13}C of the solvent, and ^{31}P NMR spectra were referenced to H_3PO_4 using the Ξ scale with the corresponding ^{1}H spectra.[33] All chemical shifts are reported in the standard δ notation in parts per million; positive chemical shifts are a higher frequency than the reference. Solution magnetic moments were determined by Evans Method using a sealed capillary containing either 5% $CHCl_3/CDCl_3$ or 5% C_6H_6/CD_3CN as internal reference.[34] Perpendicular-mode X-band electron paramagnetic resonance (EPR) spectra were collected using a Bruker EMX spectrometer. Infrared (IR) absorption measurements were taken as thin films or compressed solids on a Thermo Scientific Nicolet iS5 spectrophotometer with an iD5 ATR attachment. Spectroelectrochemical experiments were performed using a 3-electrode cell with platinum working, silver reference, and platinum counter electrodes.[35] Background spectra were taken before electrolysis, and difference spectra were collected while applying a controlled potential. For each experiment, potentials were measured and applied relative to an internal ferrocene reference. Electrochemical experiments were carried out with a Biologic VSP-300 potentiostat or a Pine Wavedriver 10 potentiostat. Electrochemical experiments were carried out in acetonitrile solutions with 1.0 mM analyte and 0.20 M Bu_4NPF_6 or Bu_4NBF_4. The working electrode was a glassy carbon disc with a diameter of 3 mm or 1 mm, the counter electrode was a glassy carbon rod, and the reference electrode was a silver wire in 0.20 M Bu_4NPF_6 or Bu_4NBF_4 in CH_3CN separated from the bulk solution by a Vycor frit. Potentials were referenced at 100 mV/s (unless otherwise noted) to the ferrocene/ferrocenium couple at 0 V using ferrocene as an internal reference. Bulk electrolysis was carried out in a 2-compartment cell separated by a fine frit, with the working electrode (vitreous carbon) and reference electrode (silver wire in 0.2 M Bu_4NPF_6 in CH_3CN separated by Vycor frit) in one compartment and the counter electrode (nichrome wire) in the other. The working compartment contained 1.0 mM **2a**, 1.0 mM ferrocene, 0.20 M Bu_4NPF_6, and 50 mM $[HDBU][BF_4]$ in acetonitrile. The counter compartment contained 1.0 mM ferrocene and 0.20 M Bu_4NPF_6. The headspace of the working compartment was sampled by syringe.

Syntheses. *$[(P^CN^CP)Co(NCCH_3)_2][BF_4]_2$ (**1a**).* Solid P^CN^CP (149.4 mg, 377.7 μmol) was added to a solution of $[Co(NCCH_3)_6][BF_4]_2$ (178.3 mg, 372.4 μmol) in 5 mL of CH_3CN. The dark orange solution was stirred at 25 °C for 15 h, and then the solvent was removed *in vacuo*. The resulting crude product was redissolved in ca. 1 mL of CH_2Cl_2 with 5 drops of CH_3CN and layered with 4 mL of Et_2O. After 1 d, the resulting rust-colored solid was isolated by filtration and washed with 2 × 4 mL THF (yield 244.2 mg, 92%). Anal. Calcd (Found) for $C_{27}H_{49}N_3B_2F_8P_2Co$ (%): C 45.66 (45.91), H 6.95 (6.89), N 5.92 (6.18). μ_{eff} (5% C_6H_6/CD_3CN, Evans method, 298 K): 2.0 μ_B. EPR (EtOH, 77 K): g_1 = 2.28, g_2 = 2.02, A_2 = 94 G.

*$[(P^NN^NP)Co(NCCH_3)_2][BF_4]_2$ (**1b**).* To a stirred orange solution of $[Co(NCCH_3)_6][BF_4]_2$ (143.4 mg, 299.5 μmol) in 8 mL of CH_3CN was added solid P^NN^NP (119.4 mg, 360.4 μmol) resulting in a dark orange solution. After stirring for 12 h at 25 °C, the solvent was removed *in vacuo*, leaving a sticky dark orange residue. The residue was dissolved in 10 mL of 1:1 toluene/CH_3CN, and the vial was placed in a larger container containing ca. 20 mL of toluene. After 2 days, the resulting dark orange crystals were decanted, washed with 2 × 2 mL THF, and dried *in vacuo* (yield 209.7 mg, 98%). Anal. Calcd (Found) for $C_{27}H_{50}N_6B_2F_8P_2Co$ (**1b**·CH_3CN) (%): C 43.05 (43.20), H 6.69 (6.56), N 11.16 (10.90). μ_{eff} (5% C_6H_6/CD_3CN, Evans method, 298 K): 2.0 μ_B. EPR (EtOH, 77 K): g_1 = 2.26, g_2 = 2.01, A_2 = 91 G.

*$[(P^ON^OP)Co(NCCH_3)_2][BF_4]_2$ (**1c**).* To a solution of $[Co(NCCH_3)_6][BF_4]_2$ (90.9 mg, 190 μmol) in 7 mL of THF with 1 mL of CH_3CN was added solid P^ON^OP (75.8 mg, 190 μmol). After stirring at 25 °C for 1 h, the dark orange solution was evaporated *in vacuo* to provide crude **2c** (yield 134.7 mg, 99%). All attempts to recrystallize **1c** resulted in partial decomposition. EPR (THF/CH_3CN, 77 K): g_1 = 2.24, g_2 = 2.00, A_2 = 85 G.

*$[(P^CN^CP)Co(NCCH_3)_2][BPh_4]_2$ (**1a′**).* A colorless solution of P^CN^CP (200.5 mg, 506.9 μmol) in 5 mL of CH_2Cl_2 was added slowly to a 5 mL blue solution of $CoBr_2$ (110.8 mg, 506.5 μmol) in CH_3CN. The solution developed a dark purple color and was stirred for 12 h. The solvent was then removed *in vacuo*. The crude product (53.6 mg) was dissolved in 5 mL of CH_2Cl_2 and 1 mL of CH_3CN and treated with $NaBPh_4$ (59.9 mg, 175 μmol). After stirring for 1 d, 15 drops of CH_3CN and 5 drops of toluene were added, and the suspension was filtered. The orange filtrate was dried *in vacuo*, producing an orange powder which was recrystallized by slow evaporation of a toluene/acetonitrile solution. This material was characterized by crystallography only.

*$[(P^CN^CP)Co(NCCH_3)][BF_4]$ (**2a**).* A dark orange solution of **1a** (123.9 mg, 174.5 μmol) in 2 mL of THF and 2 mL of CH_3CN was frozen in a cold well and then allowed to thaw. To the just-thawed solution was added solid KC_8 (24.3 mg, 178 μmol), resulting in an immediate color change to dark green. After stirring at room temperature for 4 h, the solution was filtered, and the solvent was removed from the filtrate affording dark green residue. The sticky solid was suspended in 6 mL of Et_2O, filtered, and washed with 4 mL of C_6H_6 and 4 mL of Et_2O. The solid was then extracted with 2 × 5 mL 4:1 C_6H_6/CH_3CN. Removal of solvent from the filtrate provided a dark green residue. Suspending in 4 mL of Et_2O and removing the solvent again provided pure **2a** as a dark green powder (yield 90.3 mg, 89%). APCI-MS (CH_3CN) *m/z*: 495.4 ($[M - BF_4]^+$), 454.4 ($[M - CH_3CN,BF_4]^+$). ^{1}H NMR (CD_3CN) δ/ppm: 7.46 (t, $^3J_{HH}$ = 7.7 Hz, 1H, aryl−H), 6.99 (d, $^3J_{HH}$ = 7.7 Hz, 2H, aryl−H), 3.11 (s, 4H, $-CH_2-$), 1.48 (s, 36H, ^{t}Bu). ^{1}H NMR (d_6-acetone) δ/ppm: 7.55 (t, $^3J_{HH}$ = 7.6 Hz, 1H, aryl−H), 7.08 (d, $^3J_{HH}$ = 7.5 Hz, 2H, aryl−H), 3.31 (s, 4H, $-CH_2-$), 1.55 (s, 36H, ^{t}Bu). ^{13}C{^{1}H} NMR (126 MHz, CD_3CN) δ/ppm: 165.0, 134.1, 122.0, 35.8, 32.7, 30.0. ^{31}P{^{1}H} NMR (162 MHz, CD_3CN) δ/ppm: 103.0 (br s, P^{t}Bu$_2$). ^{31}P{^{1}H} NMR (162 MHz, d_6-acetone) δ/ppm: 69.3 (br s, P^{t}Bu$_2$). IR (solid) $\bar{\upsilon}_{max}/cm^{-1}$: 2229 (C≡N).

dx.doi.org/10.1021/ic5021725 | Inorg. Chem. 2014, 53, 13031−13041

*[(P^{N}N^{N}P)Co(NCCH$_3$)][BF$_4$] (**2b**).* A dark orange solution of **1b** (110.1 mg, 155.3 μmol) in 4 mL of THF and 1.5 mL of CH_3CN was frozen in a cold well and then allowed to thaw. To the just-thawed solution was added solid KC_8 (21.2 mg, 155 μmol, 1 equiv), resulting in an immediate color change to dark purple. After stirring at room temperature for 1.5 h, 2 mL of toluene was added, and the solution was filtered. Removal of solvent from the filtrate provided **2b** (yield 84.4 mg, 93%). Anal. Calcd (Found) for $C_{23}H_{44}N_4BF_4P_2Co$ (%): C 47.28 (47.50), H 7.59 (7.39), N 9.59 (9.36). APCI-MS (CH_3CN) *m*/*z*: 497.4 ([M − BF_4]$^+$), 456.3 ([M − CH_3CN,BF_4]$^+$). ^{1}H NMR (CD_3CN) δ/ppm: 7.16 (t, $^3J_{HH}$ = 8.0 Hz, 1H, aryl−H), 6.48 (br s, 2H, −NH−), 6.01 (d, $^3J_{HH}$ = 8.0 Hz, 2H, aryl−H), 1.47 (br vt, 36H, ^{t}Bu). ^{13}C{^{1}H} NMR (126 MHz, CD_3CN) δ/ppm: 165.0, 138.1, 97.7, 38.8, 28.8. ^{31}P{^{1}H} NMR (162 MHz, CD_3CN) δ/ppm: 121.0 (br s, P^{t}Bu$_2$). IR (solid) $\bar{\upsilon}_{max}$/cm^{-1}: 3324 (N—H), 2213 (C≡N).

*[(P^{O}N^{O}P)Co(NCCH$_3$)][BF$_4$] (**2c**).* [Co(NCCH$_3$)$_6$][BF$_4$]$_2$ (192.8 mg, 402.6 μmol) was dissolved in 2 mL of CH_3CN. To this solution was added P^{O}N^{O}P (160.8 mg, 402.5 μmol) as a 4 mL THF solution. After stirring at ambient temperature for 70 min, the dark orange reaction was frozen in a cold well. Immediately upon thawing, solid KC_8 (57.8 mg, 423 μmol) was added, causing an immediate color change to dark purple. After stirring at ambient temperature for 2.5 h, the reaction was filtered, separating a gray solid which was extracted with 2 × 1 mL of THF. Removal of the solvent *in vacuo* provided a sticky dark purple solid, which was suspended in 4 mL of C_6H_6 and dried again. The product was then isolated by suspending in 4 mL of C_6H_6, filtering, and drying the solid under vacuum (yield 170.2 mg, 72%). APCI-MS (CH_3CN) *m*/*z*: 499.3 ([M − BF_4]$^+$), 458.3 ([M − CH_3CN,BF_4]$^+$). ^{1}H NMR (CD_3CN) δ/ppm: 7.67 (t, $^3J_{HH}$ = 8.1 Hz, 1H, aryl−H), 6.55 (d, $^3J_{HH}$ = 8.1 Hz, 2H, aryl−H), 1.56 (s, 36H, ^{t}Bu). ^{13}C{^{1}H} NMR (126 MHz, CD_3CN) δ/ppm: 167.8, 140.9, 102.9, 40.9, 28.0. ^{31}P{^{1}H} NMR (162 MHz, CD_3CN) δ/ppm: 214.2 (br s, P^{t}Bu$_2$). IR (solid) $\bar{\upsilon}_{max}$/cm^{-1}: 2250 (C≡N).

*Reaction of [(P^{C}N^{C}P)Co(NCCH$_3$)][BF$_4$] (**2a**) with CO.* In an NMR tube capped with a septum, a CD_3CN solution of **2a** was bubbled with CO gas for 2 min resulting in a color change from dark green to orange. ^{1}H NMR (CD_3CN) δ/ppm: 7.72 (t, $^3J_{HH}$ = 7.8 Hz, 1H, aryl−H), 7.36 (d, $^3J_{HH}$ = 7.8 Hz, 2H, aryl−H), 3.86 (vt, 4H, −CH_2−), 1.42 (vt, 36H, ^{t}Bu). ^{13}C{^{1}H} NMR (126 MHz, CD_3CN) δ/ppm: 202.6, 162.3, 139.4, 122.4 (t, *J* = 5.0 Hz), 38.8 (t, *J* = 8.3 Hz), 37.8 (t, *J* = 9.8 Hz), 29.5. ^{31}P{^{1}H} NMR (162 MHz, CD_3CN) δ/ppm: 106.3 (br s, P^{t}Bu$_2$). IR (thin film) $\bar{\upsilon}_{max}$/cm^{-1}: 1911 (C≡O). IR (CH_3CN solution, 0.2 M Bu_4NBF_4) $\bar{\upsilon}_{max}$/cm^{-1}: 1920 (C≡O).

*Reaction of [(P^{N}N^{N}P)Co(NCCH$_3$)][BF$_4$] (**2b**) with CO.* In an NMR tube capped with a septum, a CD_3CN solution of **2b** was bubbled with CO gas for 2 min resulting in a color change from dark purple to green. ^{1}H NMR (CD_3CN) δ/ppm: 7.45 (br t, 1H, aryl−H), 6.92 (br s, 2H, −NH−), 6.35 (d, $^3J_{HH}$ = 8.1 Hz, 2H, aryl−H), 1.44 (vt, 36H, ^{t}Bu). ^{31}P{^{1}H} NMR (162 MHz, CD_3CN) δ/ppm: 158.9 (br s), 142.2 (br s). IR (thin film) $\bar{\upsilon}_{max}$/cm^{-1}: 3303 (N−H), 1923 (C≡O), 1877 (weak).

*Reaction of [(P^{O}N^{O}P)Co(NCCH$_3$)][BF$_4$] (**2c**) with CO.* In an NMR tube capped with a septum, a CD_3CN solution of **2c** was bubbled with CO gas for 2 min resulting in a color change from dark purple to dark yellow-green. ^{1}H NMR (CD_3CN) δ/ppm: 8.10 (br t, aryl−H), 7.95 (br t, aryl−H), 6.99 (m, aryl−H), 1.54 (br, ^{t}Bu). ^{31}P{^{1}H} NMR (162 MHz, CD_3CN) δ/ppm: 238.1 (br s), 229.7 (br s). IR (thin film) $\bar{\upsilon}_{max}$/cm^{-1}: 1936 (C≡O), 1901 (weak).

Computational Methods. The free energies of organometallic species were calculated using

$$G_{298K} = E_{elec} + G_{solv} + ZPE + H_{vib} + nkT/2 - T(S_{elec} + S_{vib})$$

where G_{solv} is the free energy of solvation, ZPE is the zero point energy correction, S_{vib} and S_{elec} are the vibrational and electronic entropies, and n = 12 accounts for the potential and kinetic energies of the translational and rotational modes. Geometry optimization and frequency calculations were performed using the B3LYP-d3 dispersion-corrected hybrid density functional[36] with the Los Alamos small core potential[37] and 3-ζ valence functions on cobalt (augmented with diffuse functions and additional *s* (α = 0.28) and *p* (α = 0.25) functions) and 6-31G** on organics.[38] (The single d-function on phosphorus was replaced by two uncontracted gaussians with exponents of 0.45 and 1.35.) Single point energies including solvation were computed using the previous 3-ζ Los Alamos basis augmented with f-functions,[39] the 6-311G**++ basis on organics,[40] and 6-311++G-3df on phosphorus.[40a,41] Solvent effects in acetonitrile were included using the PBF implicit solvation model[42] using a dielectric constant of 37.5 and probe radius of 2.19 Å. To determine accurate free energies for solvent molecules, the 1 atm ideal gas free energy of acetonitrile was computed using the appropriate statistical mechanics formulas, and the empirical free energy of vaporization (1.27 kcal/mol, derived from the vapor pressure)[43] was subtracted. The chemical potential of H^+ (1 M) in CH_3CN was the ideal gas free energy ($H - TS = {}^5/_2kT$ − (298 K)(26.04 e.u.)[44] = −6.3 kcal/mol) minus the free energy of hydration (Δ*G*(1 atm → 1 M) = 264.0 kcal/mol)[45] plus the transfer free energy (Δ*G*(1 M, aq → 1 M, CH_3CN) = 5.7 kcal/mol).[46] All calculations were completed with Jaguar.[47]

The formally "Co(0)" solvent complexes are best described as high spin, cationic Co(I) centers antiferromagnetically coupled to radical anionic pyridine ligands. The approximate projection scheme proposed by Yamaguchi[48] was applied (using the large basis, unsolvated wave functions) to correct electronic energies of the unrestricted doublets for spin-contamination from the higher-energy quartet state. S^2 values of the broken-symmetry doublets ranged from 1.50 to 1.65, leading to corrections of up to 3.2 kcal/mol. Wave functions for Co(II) and Co(I) states did not suffer spin contamination.

■ ASSOCIATED CONTENT

Ⓢ Supporting Information

CIF files (CCDC deposition numbers) for **1a** (1022629), **1a′** (1022631), **1b** (1022633), **2a** (1022630), and **2b** (1022632). Additional crystallographic data, cyclic voltammograms, ^{1}H NMR spectra, and computational data. This material is available free of charge via the Internet at http://pubs.acs.org.

■ AUTHOR INFORMATION

Corresponding Author

*E-mail: j.yang@uci.edu.

Notes

The authors declare no competing financial interest.

■ ACKNOWLEDGMENTS

This material is based upon work performed at the Joint Center for Artificial Photosynthesis, a DOE Energy Innovation Hub, supported through the Office of Science of the U.S. Department of Energy under Award Number DE-SC0004993, and additional support from the School of Physical Sciences at the University of California, Irvine. S.I.J. would like to acknowledge support from the National Science Foundation Graduate Research Fellowship under Grant DGE# 1144469. The authors thank C. Tsay and L. Henling for helpful discussions and assistance.

■ REFERENCES

(1) (a) Gray, H. B. *Nat. Chem.* **2009**, *1* (1), 7−7. (b) Harriman, A. *Philos. Trans. R. Soc., A* **2013**, *371* (1996), 1−16. (c) Lewis, N. S.; Nocera, D. G. *Proc. Natl. Acad. Sci. U.S.A.* **2006**, *103* (43), 15729−15735. (d) DuBois, D. L. *Inorg. Chem.* **2014**, *53* (8), 3935−3960. (e) Rakowski Dubois, M.; Dubois, D. L. *Acc. Chem. Res.* **2009**, *42* (12), 1974−1982. (f) Whipple, D. T.; Kenis, P. J. A. *J. Phys. Chem. Lett.* **2010**, *1* (24), 3451−3458. (g) Appel, A. M.; Bercaw, J. E.; Bocarsly, A. B.; Dobbek, H.; DuBois, D. L.; Dupuis, M.; Ferry, J. G.; Fujita, E.; Hille, R.; Kenis, P. J. A.; Kerfeld, C. A.; Morris, R. H.; Peden, C. H. F.; Portis, A. R.; Ragsdale, S. W.; Rauchfuss, T. B.; Reek, J. N. H.; Seefeldt, L. C.; Thauer, R. K.; Waldrop, G. L. *Chem. Rev.* **2013**, *113* (8), 6621−

6658. (h) Qiao, J.; Liu, Y.; Hong, F.; Zhang, J. *Chem. Soc. Rev.* **2014**, *43* (2), 631−675. (i) Kondratenko, E. V.; Mul, G.; Baltrusaitis, J.; Larrazabal, G. O.; Perez-Ramirez, J. *Energy Environ. Sci.* **2013**, *6* (11), 3112−3135. (j) Inglis, J. L.; MacLean, B. J.; Pryce, M. T.; Vos, J. G. *Coord. Chem. Rev.* **2012**, *256* (21−22), 2571−2600. (k) Benson, E. E.; Kubiak, C. P.; Sathrum, A. J.; Smieja, J. M. *Chem. Soc. Rev.* **2009**, *38* (1), 89−99.

(2) (a) Wang, M.; Chen, L.; Sun, L. *Energy Environ. Sci.* **2012**, *5* (5), 6763−6778. (b) Yang, J. Y.; Bullock, R. M.; DuBois, M. R.; DuBois, D. L. *MRS Bull.* **2011**, *36* (01), 39−47. (c) Thoi, V. S.; Sun, Y.; Long, J. R.; Chang, C. J. *Chem. Soc. Rev.* **2013**, *42* (6), 2388−2400. (d) McKone, J. R.; Marinescu, S. C.; Brunschwig, B. S.; Winkler, J. R.; Gray, H. B. *Chem. Sci.* **2014**, *5* (3), 865−878.

(3) (a) Rofer-DePoorter, C. K. *Chem. Rev.* **1981**, *81* (5), 447−474. (b) Khodakov, A. Y.; Chu, W.; Fongarland, P. *Chem. Rev.* **2007**, *107* (5), 1692−1744.

(4) (a) Morris, A. J.; Meyer, G. J.; Fujita, E. *Acc. Chem. Rev.* **2009**, *42* (12), 1983−1994. (b) Kumar, B.; Llorente, M.; Froehlich, J.; Dang, T.; Sathrum, A.; Kubiak, C. P. *Annu. Rev. Phys. Chem.* **2012**, *63* (1), 541−569.

(5) (a) Bligaard, T.; Nørskov, J. K.; Dahl, S.; Matthiesen, J.; Christensen, C. H.; Sehested, J. *J. Catal.* **2004**, *224* (1), 206−217. (b) Ichikawa, S. *Chem. Eng. Sci.* **1990**, *45* (2), 529−535. (c) Parsons, R. Volcano Curves in Electrochemistry. In *Catalysis in Electrochemistry*; John Wiley & Sons, Inc.: New York, 2011; pp 1−15.

(6) (a) Giannoccaro, P.; Vasapollo, G.; Nobile, C. F.; Sacco, A. *Inorg. Chim. Acta* **1982**, *61*, 69−75. (b) Khaskin, E.; Diskin-Posner, Y.; Weiner, L.; Leitus, G.; Milstein, D. *Chem. Commun.* **2013**, *49* (27), 2771−2773. (c) Dahlhoff, W. V.; Nelson, S. M. *J. Chem. Soc. A* **1971**, 2184−2190. (d) Semproni, S. P.; Milsmann, C.; Chirik, P. J. *J. Am. Chem. Soc.* **2014**, *136*, 9211−9224.

(7) Semproni, S. P.; Hojilla Atienza, C. C.; Chirik, P. J. *Chem. Sci.* **2014**, *5* (5), 1956−1960.

(8) Obligacion, J. V.; Semproni, S. P.; Chirik, P. J. *J. Am. Chem. Soc.* **2014**, *136* (11), 4133−4136.

(9) (a) Müller, G.; Klinga, M.; Leskelä, M.; Rieger, B. *Z. Anorg. Allg. Chem.* **2002**, *628* (13), 2839−2846. (b) Chen, L.; Ai, P.; Gu, J.; Jie, S.; Li, B.-G. *J. Organomet. Chem.* **2012**, *716* (0), 55−61.

(10) DuBois, D. L.; Miedaner, A.; Haltiwanger, R. C. *J. Am. Chem. Soc.* **1991**, *113* (23), 8753−8764.

(11) (a) Simpson, T. C.; Durand, R. R., Jr. *Electrochim. Acta* **1988**, *33* (4), 581−583. (b) Arana, C.; Yan, S.; Keshavarz-K, M.; Potts, K. T.; Abruna, H. D. *Inorg. Chem.* **1992**, *31* (17), 3680−3682. (c) Chiericato, G., Jr.; Arana, C. R.; Casado, C.; Cuadrado, I.; Abruña, H. D. *Inorg. Chim. Acta* **2000**, *300*−*302*, 32−42. (d) Hossain, A. G. M. M.; Nagaoka, T.; Ogura, K. *Electrochim. Acta* **1997**, *42* (16), 2577−2585. (e) Fisher, B. J.; Eisenberg, R. *J. Am. Chem. Soc.* **1980**, *102* (24), 7361−7363. (f) Pearce, D. J.; Pletcher, D. *J. Electroanal. Chem. Interfacial Electrochem.* **1986**, *197* (1−2), 317−330. (g) Isse, A. A.; Gennaro, A.; Vianello, E.; Floriani, C. *J. Mol. Catal.* **1991**, *70* (2), 197−208. (h) Grodkowski, J.; Neta, P.; Fujita, E.; Mahammed, A.; Simkhovich, L.; Gross, Z. *J. Phys. Chem. A* **2002**, *106* (18), 4772−4778. (i) Ogata, T.; Yanagida, S.; Brunschwig, B. S.; Fujita, E. *J. Am. Chem. Soc.* **1995**, *117* (25), 6708−6716. (j) Tinnemans, A. H. A.; Koster, T. P. M.; Thewissen, D. H. M. W.; Mackor, A. *Recl. Trav. Chim. Pays-Bas* **1984**, *103* (10), 288−295. (k) Ogata, T.; Yamamoto, Y.; Wada, Y.; Murakoshi, K.; Kusaba, M.; Nakashima, N.; Ishida, A.; Takamuku, S.; Yanagida, S. *J. Phys. Chem.* **1995**, *99* (31), 11916−11922. (l) Lacy, D. C.; McCrory, C. C. L.; Peters, J. C. *Inorg. Chem.* **2014**, *53* (10), 4980−4988.

(12) Scheuermann, M. L.; Semproni, S. P.; Pappas, I.; Chirik, P. J. *Inorg. Chem.* **2014**, *53* (18), 9463−9465.

(13) (a) Laitar, D. S.; Müller, P.; Sadighi, J. P. *J. Am. Chem. Soc.* **2005**, *127* (49), 17196−17197. (b) Chakraborty, S.; Zhang, J.; Krause, J. A.; Guan, H. *J. Am. Chem. Soc.* **2010**, *132* (26), 8872−8873. (c) Eisenschmid, T. C.; Eisenberg, R. *Organometallics* **1989**, *8* (7), 1822−1824. (d) Thammavongsy, Z.; Seda, T.; Zakharov, L. N.; Kaminsky, W.; Gilbertson, J. D. *Inorg. Chem.* **2012**, *51* (17), 9168−9170.

(14) Schneider, J.; Jia, H.; Muckerman, J. T.; Fujita, E. *Chem. Soc. Rev.* **2012**, *41* (6), 2036−2051.

(15) Addison, A. W.; Rao, T. N.; Reedijk, J.; van Rijn, J.; Verschoor, G. C. *J. Chem. Soc., Dalton Trans.* **1984**, No. 7, 1349−1356.

(16) Kundu, S.; Brennessel, W. W.; Jones, W. D. *Inorg. Chem.* **2011**, *50* (19), 9443−9453.

(17) Nelson, S. M.; D, W. V. *J. Chem. Soc. A* **1971**, No. 13, 2184−2190.

(18) Khaskin, E.; Diskin-Posner, Y.; Weiner, L.; Leitus, G.; Milstein, D. *J. Chem. Soc., Chem. Commun.* **2013**, *49* (27), 2771−2773.

(19) Jitaru, M. *J. Univ. Chem. Technol. Metall.* **2007**, *42* (4), 333−344.

(20) Zanello, P. *Inorganic Electrochemistry: Theory, Practice, and Applications*; The Royal Society of Chemistry: Cornwall, U.K., 2003.

(21) (a) DuBois, D. L. Electrochemical Reactions of Carbon Dioxide. In *Encyclopedia of Electrochemistry, Vol 7A, Inorganic Chemistry*; Bard, A. J. Stratmann, M.; Scholz, F.; Pickett, C. J., Eds.; Wiley-VCH: New York, 2006. (b) Schmidt, M. H.; Miskelly, G. M.; Lewis, N. S. *J. Am. Chem. Soc.* **1990**, *112* (9), 3420−3426.

(22) (a) Lee, G. R.; Maher, J. M.; Cooper, N. J. *J. Am. Chem. Soc.* **1987**, *109* (10), 2956−2962. (b) Chatt, J.; Kubota, M.; Leigh, G. J.; March, F. C.; Mason, R.; Yarrow, D. J. *J. Chem. Soc., Chem. Commun.* **1974**, No. 24, 1033−1034. (c) Karsch, H. H. *Chem. Ber.* **1977**, *110* (6), 2213−2221. (d) Evans, G. O.; Walter, W. F.; Mills, D. R.; Streit, C. A. *J. Organomet. Chem.* **1978**, *144* (2), C34−C38. (e) Maher, J. M.; Cooper, N. J. *J. Am. Chem. Soc.* **1980**, *102* (25), 7604−7606. (f) Carmona, E.; Gonzalez, F.; Poveda, M. L.; Marin, J. M.; Atwood, J. L.; Rogers, R. D. *J. Am. Chem. Soc.* **1983**, *105* (10), 3365−3366. (g) Alvarez, R.; Carmona, E.; Poveda, M. L.; Sanchez-Delgado, R. *J. Am. Chem. Soc.* **1984**, *106* (9), 2731−2732. (h) Bianchini, C.; Mealli, C.; Meli, A.; Sabat, M. *Inorg. Chem.* **1984**, *23* (18), 2731−2732. (i) Fachinetti, G.; Floriani, C.; Chiesi-Villa, A.; Guastini, C. *J. Am. Chem. Soc.* **1979**, *101* (7), 1767−1775. (j) Fujita, E.; Szalda, D. J.; Creutz, C.; Sutin, N. *J. Am. Chem. Soc.* **1988**, *110* (14), 4870−4871. (k) Hammouche, M.; Lexa, D.; Momenteau, M.; Saveant, J. M. *J. Am. Chem. Soc.* **1991**, *113* (22), 8455−8466. (l) Machan, C. W.; Chabolla, S. A.; Yin, J.; Gilson, M. K.; Tezcan, F. A.; Kubiak, C. P. *J. Am. Chem. Soc.* **2014**, *136* (41), 14598−14607.

(23) Hansen, H. A.; Varley, J. B.; Peterson, A. A.; Nørskov, J. K. *J. Phys. Chem. Lett.* **2013**, *4* (3), 388−392.

(24) Kaljurand, I.; Kütt, A.; Sooväli, L.; Rodima, T.; Mäemets, V.; Leito, I.; Koppel, I. A. *J. Org. Chem.* **2005**, *70* (3), 1019−1028.

(25) Rail, M. D.; Berben, L. A. *J. Am. Chem. Soc.* **2011**, *133* (46), 18577−18579.

(26) (a) Mandal, S.; Shikano, S.; Yamada, Y.; Lee, Y.-M.; Nam, W.; Llobet, A.; Fukuzumi, S. *J. Am. Chem. Soc.* **2013**, *135* (41), 15294−15297. (b) Marinescu, S. C.; Winkler, J. R.; Gray, H. B. *Proc. Natl. Acad. Sci. U.S.A.* **2012**, *109* (38), 15127−15131. (c) Wiedner, E. S.; Roberts, J. A. S.; Dougherty, W. G.; Kassel, W. S.; DuBois, D. L.; Bullock, R. M. *Inorg. Chem.* **2013**, *52* (17), 9975−9988.

(27) Izutsu, K. *Acid-Base Dissociation Constants in Dipolar Aprotic Solvents*; Blackwell: Oxford, 1990; Vol. 35.

(28) Kütt, A.; Rodima, T.; Saame, J.; Raamat, E.; Mäemets, V.; Kaljurand, I.; Koppel, I. A.; Garlyauskayte, R. Y.; Yagupolskii, Y. L.; Yagupolskii, L. M.; Bernhardt, E.; Willner, H.; Leito, I. *J. Org. Chem.* **2010**, *76* (2), 391−395.

(29) Kütt, A.; Rodima, T.; Saame, J.; Raamat, E.; Mäemets, V.; Kaljurand, I.; Koppel, I. A.; Garlyauskayte, R. Y.; Yagupolskii, Y. L.; Yagupolskii, L. M.; Bernhardt, E.; Willner, H.; Leito, I. *J. Org. Chem.* **2011**, *76* (2), 391−395.

(30) (a) Becica, J.; Jackson, A. B.; Dougherty, W. G.; Kassel, W. S.; West, N. M. *J. Chem. Soc., Dalton Trans.* **2014**, *43* (23), 8738−8748. (b) Jackson, A. B.; Schauer, C. K.; White, P. S.; Templeton, J. L. *J. Am. Chem. Soc.* **2007**, *129* (35), 10628−10629. (c) Zecchin, S.; Zotti, G.; Pilloni, G. *Inorg. Chim. Acta* **1979**, *33*, L117−L118.

(31) (a) Aresta, M.; Nobile, C. F.; Albano, V. G.; Forni, E.; Manassero, M. *Chem. Commun.* **1975**, No. 15, 636−637. (b) Aresta, M.; Nobile, C. F. *J. Chem. Soc., Dalton Trans.* **1977**, No. 7, 708−711. (c) Herskovitz, T. *J. Am. Chem. Soc.* **1977**, *99* (7), 2391−2392.

(32) (a) Hathaway, B. J.; Underhill, A. E. *J. Chem. Soc.* **1960**, 3705−3711. (b) Hathaway, B. J.; Holah, D. G.; Underhill, A. E. *J. Chem. Soc.* **1962**, 2444−2448. (c) Kawatsura, M.; Hartwig, J. F. *Organometallics* **2001**, *20* (10), 1960−1964. (d) Benito-Garagorri, D.; Becker, E.; Wiedermann, J.; Lackner, W.; Pollak, M.; Mereiter, K.; Kisala, J.; Kirchner, K. *Organometallics* **2006**, *25* (8), 1900−1913. (e) Bernskoetter, W. H.; Hanson, S. K.; Buzak, S. K.; Davis, Z.; White, P. S.; Swartz, R.; Goldberg, K. I.; Brookhart, M. *J. Am. Chem. Soc.* **2009**, *131* (24), 8603−8613.
(33) Harris, R. K.; Becker, E. D.; Cabral de Menezes, S. M.; Goodfellow, R.; Granger, P. *Pure Appl. Chem.* **2001**, *73* (11), 1795−1818.
(34) (a) Evans, D. F. *J. Chem. Soc.* **1959**, 2003−2005. (b) Schubert, E. M. *J. Chem. Educ.* **1992**, *69* (1), 62. (c) Grant, D. H. *J. Chem. Educ.* **1995**, *72* (1), 39. (d) Bain, G. A.; Berry, J. F. *J. Chem. Educ.* **2008**, *85* (4), 532.
(35) Zavarine, I. S.; Kubiak, C. P. *J. Electroanal. Chem.* **2001**, *495* (2), 106−109.
(36) (a) Becke, A. D. *J. Chem. Phys.* **1993**, *98* (7), 5648−5652. (b) Lee, C. T.; Yang, W. T.; Parr, R. G. *Phys. Rev. B* **1988**, *37* (2), 785−789.
(37) Hay, P. J.; Wadt, W. R. *J. Chem. Phys.* **1985**, *82* (1), 299−310.
(38) (a) Francl, M. M.; Pietro, W. J.; Hehre, W. J.; Binkley, J. S.; Gordon, M. S.; Defrees, D. J.; Pople, J. A. *J. Chem. Phys.* **1982**, *77* (7), 3654−3665. (b) Hehre, W. J.; Ditchfie, R.; Pople, J. A. *J. Chem. Phys.* **1972**, *56* (5), 2257−2261.
(39) Martin, J. M. L.; Sundermann, A. *J. Chem. Phys.* **2001**, *114* (8), 3408−3420.
(40) (a) Clark, T.; Chandrasekhar, J.; Spitznagel, G. W.; Schleyer, P. V. *J. Comput. Chem.* **1983**, *4* (3), 294−301. (b) Krishnan, R.; Binkley, J. S.; Seeger, R.; Pople, J. A. *J. Chem. Phys.* **1980**, *72* (1), 650−654.
(41) (a) Frisch, M. J.; Pople, J. A.; Binkley, J. S. *J. Chem. Phys.* **1984**, *80* (7), 3265−3269. (b) McLean, A. D.; Chandler, G. S. *J. Chem. Phys.* **1980**, *72* (10), 5639−5648.
(42) Tannor, D. J.; Marten, B.; Murphy, R.; Friesner, R. A.; Sitkoff, D.; Nicholls, A.; Ringnalda, M.; Goddard, W. A.; Honig, B. *J. Am. Chem. Soc.* **1994**, *116* (26), 11875−11882.
(43) (a) Putnam, W. E.; McEachern, D. M. J.; Kilpatrick, J. E. *J. Chem. Phys.* **1965**, *42*, 749−755. (b) Dojcansky, J.; Heinrich, J. *Chem. Zvesti* **1974**, *28* (2), 157−159.
(44) Chase, M. W. J. *NIST-JANAF Thermochemical Tables*, 4th ed.; NIST: Gaithersburg, MD, 1998.
(45) Tissandier, M. D.; Cowen, K. A.; Feng, W. Y.; Gundlach, E.; Cohen, M. H.; Earhart, A. D.; Coe, J. V.; Tuttle, T. R. *J. Phys. Chem. A* **1998**, *102* (40), 7787−7794.
(46) Kelly, C. P.; Cramer, C. J.; Truhlar, D. G. *J. Phys. Chem. B* **2007**, *111* (2), 408−422.
(47) Bochevarov, A. D.; Harder, E.; Hughes, T. F.; Greenwood, J. R.; Braden, D. A.; Philipp, D. M.; Rinaldo, D.; Halls, M. D.; Zhang, J.; Friesner, R. A. *Int. J. Quantum Chem.* **2013**, *113* (18), 2110−2142.
(48) Kitagawa, Y.; Saito, T.; Ito, M.; Shoji, M.; Koizumi, K.; Yamanaka, S.; Kawakami, T.; Okumura, M.; Yamaguchi, K. *Chem. Phys. Lett.* **2007**, *442* (4−6), 445−450.